Developments in the Built Environment 24 (2025) 100785

Contents lists available at ScienceDirect

Developments in the Built Environment

journal homepage: www.sciencedirect.com/journal/developments-in-the-built-environment

Evaluating the influence of synthetic cotton textile waste fibres on CO_2 uptake, flexural strength, and wet-dry ageing of slag-based binders

Anabel Castillo-Rodríguez [a], Antonia Pacios-Álvarez [b,*], João Castro-Gomes [c], Justo García-Navarro [a]

[a] Dep. Ingeniería Agroforestal, Universidad Politécnica de Madrid, Spain
[b] Dep. Sistemas Aeroespaciales, Transporte Aéreo y Aeropuertos, Universidad Politécnica de Madrid, Spain
[c] Centre of Materials and Building Technologies (C–MADE), Department of Civil Engineering and Architecture, University of Beira Interior, Portugal

ARTICLE INFO

Keywords:
Waste synthetic cotton fibres
EAFS
Accelerated carbonation
Fibre-reinforced binders
CO_2 uptake
Slag-based binders
Wet-dry ageing cycles

ABSTRACT

The construction sector is seeking sustainable alternatives to reduce CO_2 emissions, with cement replacement being a key strategy. Mineralised steel slag is a promising binder due to its reactive CaO and MgO content, enabling CO_2 sequestration via accelerated carbonation while maintaining mechanical performance. Incorporating textile waste cotton fibres offers complementary benefits, enhancing flexural strength and potentially increasing CO_2 uptake through improved porosity and carbonation pathways. Given the global textile waste surplus and low recycling rates, this approach supports circular economy goals. This study examines composites combining carbonated steel slag with synthetic cotton fibres at three dosages, assessing carbonation uptake and flexural strength under standard curing and wet–dry ageing cycles. Results indicate that fibres promote higher CO_2 uptake by creating diffusion channels and improve mechanical behaviour, particularly at higher dosages. Although durability cycles reduce toughness, they enhance environmental performance by facilitating greater carbonation.

1. Introduction

Cement is the primary binder in concrete and the major contributor to CO_2 emissions in construction. To mitigate its environmental impact, the sector is advancing by improving the sustainability of cement production and developing alternative binders. The industry is optimising processes, shifting to renewable energy and incorporating supplementary cementitious materials (SCMs) such as fly ash, silica fume, blast furnace slag, metakaolin, and others derived from industrial or agricultural waste. These materials not only act as fillers, but also exhibit pozzolanic activity, enhancing thermal stability and mechanical performance (Park and Lee, 2024) (Assi et al., 2018).

Efforts have also focused on developing cement-free binders through alkali activation and carbonation. The properties of alkali-activated binders are influenced by the composition of the raw material and the type and concentration of the activating solution. Sodium and potassium hydroxides, sometimes combined with water glass, are typical activators, and higher alkali concentrations generally yield stronger materials. Despite promising mechanical performance, especially at high temperatures, geopolymers face scalability and cost challenges, particularly because of sodium hydroxide availability. These developments suggest that geopolymers and other alternative binders could support structural applications, especially in high-temperature environments, offering a pathway to reduce the use of Portland cement.

Steel slag presents a viable path to reduce the dependence on Portland cement, addressing both carbon capture and sustainable construction material development. Steel slag, a by-product of basic oxygen furnace (BOF) and electric arc furnace (EAF) steelmaking, contains reactive phases such as free CaO, MgO, and C_2S, C_3S that readily react with CO_2 to form carbonates such as $CaCO_3$ and $MgCO_3$. These carbonation reactions are exothermic and thermodynamically favourable, mimicking natural weathering, but significantly accelerated under controlled conditions (DiGiovanni et al., 2024) (Huang et al., 2024) (Biava et al., 2024). Carbonated steel slag can sequester substantial amounts of CO_2: studies estimate CO_2 uptake capacities of up to 130–330 g of CO_2 per kg of slag depending on process parameters (Biava et al., 2024), (Woodall et al., 2019). Carbonated steel slag is being valorised in several applications: a) as a supplementary cementitious

* Corresponding author.
E-mail address: antonia.pacios@upm.es (A. Pacios-Álvarez).

https://doi.org/10.1016/j.dibe.2025.100785
Received 11 August 2025; Received in revised form 9 October 2025; Accepted 21 October 2025
Available online 22 October 2025

material (SCM), replacing a portion of Portland cement; b) as fine or coarse aggregate in concrete; c) in novel binders such as carbonated reactive magnesia cement (CRMC), incorporating additional waste streams while maintaining compressive strengths up to 14.6 MPa after 24 h curing (Grünhäuser Soares et al., 2022).

Another important source of waste materials, textile waste, has become a critical environmental issue worldwide. Every year, approximately 92 million tonnes of textile waste are generated globally, a number projected to increase to 134 million tonnes by 2030 if current trends continue (Key et al., 2023) (Chen et al., 2021). For example, the EU-27 generated approximately 6.95 million tons of textile waste in 2020 (16 kg per person), and the United States discarded ~11.3 million tons in 2018 (~37 kg per person) (Chen et al., 2021). Clothing and footwear constitute the largest waste category, about 75 % of EU textile waste (5.2 Mt) in 2020 came from apparel, with the remainder from household textiles (e.g. linens, carpets) and technical textiles (e.g. industrial fabrics, workwear). Unsold or unworn textiles add to the waste: an estimated 4–9 % of textiles in Europe are destroyed before ever reaching consumers, translating to 0.26–0.59 Mt wasted annually (Agency, 2024). This linear model has made textiles a major environmental burden, linked to 10 % of global carbon emissions and extensive use of resources.

Current recycling rates for textiles are low. In general, only around 12–15 % of textile waste is recycled in any form and less than 1 % of the used clothing is actually recycled into new garments. In the EU, for example, only 22 % of post-consumer textiles are collected separately for reuse or recycling, with the rest often landfilled or incinerated. The United Kingdom manages to recycle about 30 % of used clothes (the remainder going to disposal), while the United States recycles only approx. 15 %. Some countries demonstrate better results, Germany recovers approx0.75 % of its textile waste for reuse/recycling, and Sweden now collects over 95 % of discarded textiles, but these are exceptions aided by efficient collection/sorting systems (Textile waste by numbers). A key distinction lies between post-consumer waste textiles discarded by end-users, and pre-consumer waste from manufacturing. Pre-consumer wastes are relatively clean and homogeneous, and their fibre composition is known, which facilitates recycling at this stage. In contrast, post-consumer textile waste is often mixed, contaminated, and harder to recycle. As a result, the vast majority, roughly 80–85 % of used textiles globally end up burned or dumped as waste (Chen et al., 2021).

Fibre type and material composition greatly influence recyclability. Textiles made from a single fibre (e.g., 100 % cotton or 100 % polyester) are much more amenable to recycling than blended fabrics. Natural fibres (cotton, wool) can be mechanically downcycled into insulation, rags, or shoddy, although fibre quality diminishes with each recycle. Synthetic polymers (polyester, nylon) can be melted or chemically recycled into new fibres, but only if collected and sorted pure. Currently, only 8 % of textile fibres used worldwide are made from recycled inputs, underscoring the need to improve circularity.

In this scenario, to address the environmental trade-offs and life cycle impacts of using carbonated slag and textile waste fibres in construction, the following research questions are posed: To what extent does the incorporation of textile waste fibres improve the carbonation of slag-based composites? And what is the synergistic potential of combining carbonated steel slag with textile fibre waste to reinforce brittle matrices?

The main objective of this work is to study influence of fibre dosage on CO_2 uptake, and the mechanical behaviour of the composites. A proven carbonation procedure was followed, so the waste textile fibre dosage and the environmental cycles exposure. The flexural strength for standard and wet-dry ageing conditions was determined; the study was completed with MIP. A comprehensive study of carbon uptake was performed by TGA and SEM-EDX analysis.

2. Literature review

As is already known, by exposing slag-bearing materials to CO_2 under various conditions, these calcium phases can be converted to stable carbonates. There are three primary direct carbonation modes for slag-derived systems: dry carbonation, where the gas reacts with dry or minimally moist solids; thin-film carbonation, where CO_2 is used to cure a humid powder or compact, where only a thin water film coats the particles and wet carbonation, where CO_2 reacts with alkaline solids in an aqueous medium (Ferrara et al., 2023). Each mode involves the same fundamental chemical conversions of the Ca-bearing phases into $CaCO_3$, but through different mechanisms and process conditions.

Dry carbonation forms a strong surface layer useful for curing concrete products, but slow diffusion limits depth; requires long time or high CO_2 to penetrate deeper. The typical CO_2 uptake is limited by surface reaction and varies from 5 to 15 wt%. Only the outer layer of the surface of the particle carbonates, whereas the core remains unreacted. Wet carbonation is the fastest and most complete carbonation (20–40 wt % under optimal conditions), especially under pressure and heat; it can completely sequester maximum CO_2, close to theoretical CO_2 capture, and eliminate free CaO/MgO (Ferrara et al., 2023), (Bonfante et al., 2024).

Thin-film carbonation has faster kinetics than dry carbonation and more complete carbonation of particles. It is suitable for CO_2 curing of precast elements (semi-dry mixes). It maintains the shape of the product and adds strength quickly, but must control moisture carefully: too wet turns to slurry, too dry behaves like dry mode. Initially, if fresh slag contains free $CaO/Ca(OH)_2$, carbonation is very rapid on the surface, creating an immediate $CaCO_3$ layer. As time progresses, CO_2 uptake slows considerably because the porosity is progressively clogged by carbonate precipitate. Moisture released by carbonation can raise local humidity, but eventually the carbonate-lined pores impede further gas diffusion, causing a self-limiting reaction.

In a thin-film, carbonation can follow two paths: a direct reaction at the solid surface (like dry mode) and a slightly deeper hydration–carbonation because moisture penetrates pores. Hydration of free CaO/C_2S occurs because the water in the film can hydrate CaO fully to $Ca(OH)_2$ and partially hydrate silicates to C–S–H: these hydrates then immediately carbonate as CO_2 dissolves in the same film. Essentially, hydration and carbonation occur simultaneously or in rapid sequence in thin-film conditions. Through a dissolution–precipitation mechanism, calcium ions (Ca^{2+}) can dissolve in the thin water layer—particularly in highly alkaline environments, and subsequently react with carbonate ions (CO_3^{2-}) in solution to precipitate calcium carbonate ($CaCO_3$), either on the original particle surface or at a short distance away. This can lead to carbonate crystals nucleating within the water film rather than strictly on the solid surface. As a result, we may get finer $CaCO_3$ crystallites distributed in the matrix. In particular, thin-film carbonation often produces a mixture of $CaCO_3$ polymorphs initially (due to slightly higher supersaturation than at dry gas–solid interfaces). Transient vaterite or aragonite may form at an early stage but typically recrystallise to calcite as the system ages and dries, which is the stable form detected in the final products. The overall reaction yield is still predominantly calcite. In summary, the chemical conversions in thin-film carbonation mirror those of dry carbonation but proceed more completely because of the improved reaction medium. All available CaO, $Ca(OH)_2$ will carbonate, and a larger fraction of Ca-silicates will eventually convert because continuous moisture allows the continuous hydration of their cores with concurrent carbonation.

Several authors provide models for the calculation of CO_2 uptake, theoretical CO_2 sequestration, and degree of carbonation, based on the high reactivity of CO_2 for materials containing α-C_2S, β-C_2S, and free MgO/CaO (Huntzinger et al., 2009). The analysis refers to calcium carbonate as the main mineralisation product of the adopted steel slag; however, it can be extended to other different carbonates, such as magnesium-based.

CO_2 uptake is defined as the amount of CO_2 absorbed by a material during carbonation. Common quantification methods include: mass gain method (Huntzinger et al., 2009); thermogravimetric analysis (TGA) (Ferrara et al., 2023); acid digestion (HCl-based release and quantification) (Ferrara et al., 2023), (Fang et al., 2022). Theoretical CO_2 sequestration represents the maximum possible CO_2 that can be sequestered, based on the full reaction of reactive oxides. To estimate theoretical CO_2 sequestration, consideration must be given to the waste composition and the extent to which the oxides are available for reaction. The model is based on the percentages of mass of oxides and subtracts carbonates and sulphates that are already present (Huntzinger et al., 2009) (Ferrara et al., 2023) (Grünhäuser Soares and Castro-Gomes, 2022). A common formulation, adapted from Steinour's equation, is used in all studies. The degree of carbonation is defined as the ratio of the actual CO_2 uptake to the theoretical potential; it quantifies how much of the carbonation potential has been realised. It is estimated by comparing the observed change in the dry mass of the theoretical material with the calculated extent of carbonation based on the composition of the pre-carbonated waste (Huntzinger et al., 2009). Most of them share the techniques and assumptions. Data are obtained by mass changes obtained by thermal gravimetric analysis and quantitative X-ray diffraction of: a) carbonate decomposition was observed in both pre- and post carbonated samples was observed in the temperature region of 500–850 °C.

Waste textile fibres have demonstrated potential as reinforcement in brittle matrices used in the construction sector. These fibres, derived from both natural (e.g., cotton, wool, jute) and synthetic (e.g., polyester, nylon, polypropylene) sources, enhance the ductility and toughness of inherently brittle materials by bridging microcracks, impeding their propagation, and distributing tensile stresses more uniformly across the matrix. Small dosages of textile fibres, ranging from 0.07 % to 2 % by volume, have been shown to significantly improve the compressive and flexural strength of cementitious composites, with recycled polypropylene carpet fibres and denim-based cotton fibres increasing compressive strength by up to 40 % and enhancing flexural strain capacity (Rahman et al., 2020). In cementitious composites, the incorporation of 30 % textile fibres increased the 28-day flexural strength by 22 % (Regazzi et al., 2016). Furthermore, the use of textile waste in the form of nonwoven fabric significantly improved the composites' toughness and post-cracking load-bearing capacity, with six layers of textile reinforcement identified as the optimal configuration (Sadrolodabaee et al., 2021a).

Textile waste fibres can also enhance the thermal and acoustic insulation performance of brittle matrices, especially in non-structural and sustainable construction applications. Their low thermal conductivity, typically ranging between 0.030 and 0.050 W/mK depending on the type and density, enables them to disrupt heat flow within the composite. For instance, incorporating jute fibres at 20 wt% yielded a thermal conductivity as low as 0.068 W/mK, while basalt fibres achieved 0.08 W/mK at the same content (Assi et al., 2018). The combination of 60 % nylon/spandex textile fragments mixed with 40 % polyurethane fragments achieved a thermal conductivity of 0.0953 W/mK (Dissanayake et al., 2018). Similarly, wool fibres at 46 % by weight reduced thermal conductivity by up to 92 % compared to reference mixes (Wijesinghe et al., 2024) (Dellagi et al., 2024). The porous and fibrous nature of textile waste improves sound absorption, especially in the mid to high frequency range (Wijesinghe et al., 2024). Rafdabaee et al. indicate that the insulation performance is influenced by fibre morphology, fabric structure, and fibre-matrix interaction. Short, crimped, or hollow fibres improve air entrapment. Adequate dispersion and interface adhesion are essential for consistent performance; nonwoven fabrics contribute to homogeneity and better fibre distribution (Sadrolodabaee et al., 2021b). Natural fibres such as cotton and wool, due to their hollow or crimped microstructure and hygroscopic nature, trap air and moisture, contributing to reduced thermal transmittance and dampened sound propagation. When integrated into matrices such as gypsum, lime, or cement, these fibres introduce porosity and microvoids that scatter and absorb sound waves and retard thermal conduction (Echeverria et al., 2019).

Few studies have explored the feasibility of using fibres to enhance the targeted transport of CO_2 within a matrix. Zhuge et al. conducted a comprehensive investigation of natural fibres embedded in cement pastes subjected to enforced carbonation, none of them being textile waste fibres (Zhuge et al., 2024). In their study, seven different types of fibres were incorporated into a cement-based matrix and exposed to accelerated carbonation. The cross-sectional profiles were analysed to assess CO_2 diffusion behaviour. The results indicated that all types of natural fibre contributed to the increase in CO_2 uptake. This enhancement is attributed to the internal porosity of the fibres, their spatial arrangement within the yarns, and the interconnected pore networks that they form. Porous natural fibre yarns introduced additional diffusion pathways, as evidenced by the continuous increase in carbonated area fraction and CO_2 uptake along the yarns compared to the bulk matrix. These findings suggest that the interconnected pore structures created by the yarns facilitate effective CO_2 transport throughout the system.

3. Materials and methodology

3.1. Component materials

Rounded particles of Electric-Arc-Furnace Slag (EAFS) were provided by the national steel industry in Maia and Aldeia de Paio Pires, Seixal, Portugal. Waste textile fibres were provided by Alcorcertex, S.L. (Spain). According to the initial information provided by the supplier, the fibres consisted of a polyester-cotton blend.

3.1.1. Mineral particle size

The mineral material was ground in a Vibratory Disc Mill RS 300 (Retsch) for 20 min with reverse function activated, resulting in powdered slag particles (S). The particle size distribution after grinding (AG) was determined by laser diffraction using a Bettersizer 2600 (Bettersize Instruments), producing a slag with D10 of 1.159 μm, D50 of 48.29 μm, and D90 of 178.2 μm. Fig. 1 presents the particle size distribution of the processed fraction.

3.1.2. Mineral oxide composition

The estimated oxide composition of the EAFS was estimated through X-Ray Fluorescence (XRF) analysis, carried out using a Fluorescence Spectrometer, Bruker S2Ranger with Dispersive Energy Detector. The EQUA-OXIDES measurement protocol was employed, using a palladium (Pd) X-ray tube. Prior to testing, the material was ground to a fine powder to ensure consistent results. These results are shown in Table 1.

The Loss on ignition (LOI) was obtained by simultaneous

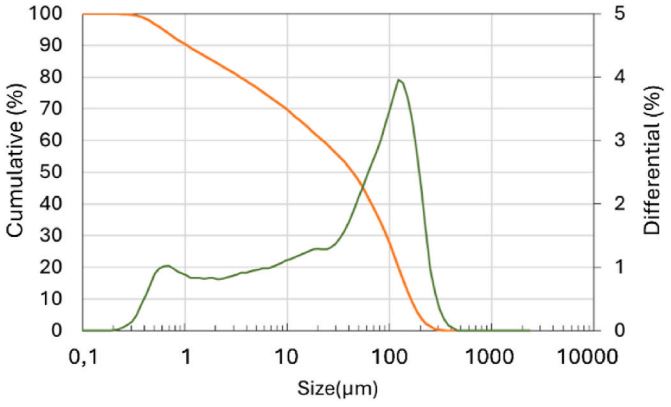

Fig. 1. Particle size distribution for the EAFS.

Table 1
Oxide composition (% wt.) and physical properties.

Chemical Properties	EAFS
CaO	31.20
Fe_2O_3	30.80
SiO_2	17.90
Al_2O_3	11.00
MgO	3.85
Cr_2O_3	2.63
MnO	0.93
TiO_2	0.69
SO_3	0.37
Loss on ignition (%)	0.72
True density (g/cm^3)	2.78

Table 2
Composition of the specimens.

CODE	S/SD	SC1/SC1D	SC2/SC2D	SC3/SC3D
w/s initial (wt.)	0.35	0.35	0.35	0.35
w/s final (wt.)	0.04	0.05	0.05	0.05
Initial EAFS (gr)	622.70	616.50	610.30	604.00
Initial water (gr)	217.94	215.77	213.60	211.40
Initial dried fibre (gr)	0.00	4.29	8.57	12.86

Thermogravimetric and Derivative Thermogravimetry analysis (TGA-DTG) using a TA Instrument SDT Q-50 apparatus and true density was determined using a gas displacement pycnometer on a Micromeritics AccuPyc 1330 pycnometer.

3.1.3. Waste textile fibres

The synthetic cotton fibres used in this study were sourced from undyed post-industrial textile waste. Fabric offcuts underwent a shredding process to recover fibres composed of a cotton–polyester blend. Fig. 2 presents the appearance of the synthetic cotton fibre fluff, together with the TGA–DTG analysis and a microscopic image.

The TGA–DTG analysis not only quantifies the mass losses but also enables the identification of the nature of the textile waste fibres incorporated into the composites. According to the TGA-DTG results (Fig. 2b), the first weight-loss stage (22–120 °C) is attributed to the evaporation of moisture from the fibres. The second stage, observed between 300 °C and 420 °C, corresponds to the thermal degradation of the textile fibres, resulting in a total weight loss of approximately 75.5 %. The degradation of cotton cellulose occurs between 320 °C and 380 °C, whereas polyester fibres begin to decompose around 380 °C and continue up to 450 °C (Wang et al., 2023), (Xia et al., 2025). The single, sharp peak centred at approximately 390 °C suggests an overlap of both degradation processes, with a predominant contribution from the cellulosic (cotton) fraction and a secondary contribution from polyester at the tail of the peak. This behaviour confirms that the textile fibres consists mainly of synthetic cotton blends containing both cellulose and polyester components. The overall loss on ignition (LOI) was 91.52 %.

Fluorescence microscopy was employed to determine the diameter of the fibres from 12 to 25 μm and lengths ranging from 11 to 44 mm (Fig. 2c). The true density, determined by AccuPyc 1330 Pycnometer of the fibre was measured as 1.91 g/cm^3 and fibres exhibited a hygroscopicity was found to be 41.48 %. Mechanical parameters were not experimentally obtained in the present study but derived from the literature to support the interpretation of the material behaviour under comparable conditions. Previous studies (Lakshmaiya et al., 2025), (Badara et al., 2025) have reported that recycled cotton and polyester fibres generally exhibit an elongation at break of 8–10 % and a tensile strength ranging from 250 to 430 MPa.

3.2. Specimens preparation

A total of eight series of specimens were cast to carry out the experimental programme. Three specimens were prepared for each series. The manufacturing procedure described in the reference study (Grünhäuser Soares et al., 2024) was adapted to enable the incorporation of waste textile fibres. To ensure traceability in the final water content, a control series was casted following the original procedure.

Due to fibre hygroscopic nature, an initial water-to-slag ratio of 35 % by weight was used to ensure homogeneous mixing and full fibre saturation. The excess water was then removed by mechanical compression, resulting in a final water-to-slag ratio that varied according to fibre incorporation, from approximately 0.04 by weight for the reference mix to 0.05 for the fibre-reinforced composites. The amount of water expelled during compression, together with the mass and volume of each specimen recorded after demoulding, were essential for accurately determining the effective water-to-slag ratio of each mix (see Table 2).

The mixtures were prepared in a laboratory mixer pan. The fresh paste was poured onto a 40 cm diameter paper filter, and excess water was manually removed until a workable consistency was achieved. The mixture was then cast into 10 × 40 × 160 mm moulds and subjected to 10 MPa of pressure using a HOLZMANN WP30PLUS hydraulic press for 5 min, as can be seen in Fig. 3a and b. Afterward, the specimens were demoulded. Due to the manufacturing process, small dimensional variations were noticed and registered to be considered in the properties' determination.

The samples underwent an accelerated carbonation curing process at 60 °C and 0.8 bar CO_2 pressure for 24 h (Fig. 3c). Then they were placed in a conventional oven at 60 °C for an additional 24 h to complete the hardening. All specimens were also measured and weighted, after carbonation, and after drying.

Four out of the eight series of specimens were subjected to durability test, with the aim of studying the effects of these processes on the specimens. The durability test consisted of applying, after curing in a CO_2 chamber, 25 wet-dry cycles according to EN 12467:2013+A2. Each wet-dry cycle consisted of drying for 6 h at a temperature of 60 °C and 60 % RH followed by 18 h of immersion in water at 20 °C.

The notation is as follow "S" refers to slag, "C" to synthetic cotton fibre, the number to the dosage percentage, and "D" to de samples

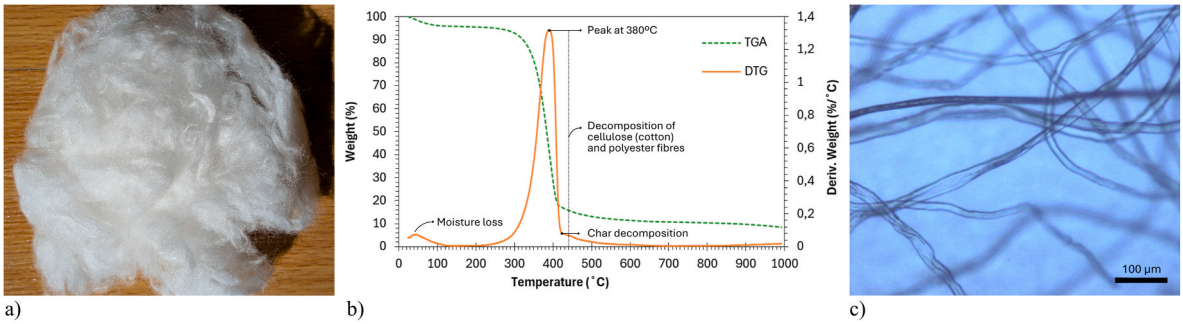

Fig. 2. Synthetic cotton waste fibres: (a) Synthetic cotton fluff; (b) TGA and DTG curves of the synthetic cotton fibres; (c) Microscopic image of SC at 10X.

a) b) c)

Fig. 3. Preparation of the samples: (a) mixing preparation; (b) compression process and removal of excess water; (c) carbonation chamber.

subjected to wet-dry cycles.

After being tested for flexural strength, samples were taken from the centre of the specimens to conduct the Thermogravimetric and Derivative Thermogravimetry analysis (TGA-DTG), Mercury Intrusion Porosimetry (MIP), X-Ray Diffraction (XRD) and Scanning Electron Microscopy (SEM) test.

3.3. Experimental programme

TGA and derivative thermogravimetric analysis (DTG) were performed with a SDT Q-50 TA instrument model, heating the material from ambient temperature (20 ± 2 °C) to 1000 °C at a rate of 20 °C/min under nitrogen flow. Before testing, approximately 5 mg of sample underwent a 24 h drying process at 60 °C. Furthermore, the loss of ignition (LOI) was determined by TGA analysis using the same SDT Q-50 (TA Instrument). The TGA analysis was also used to estimate the amount of CO_2 uptake (UCO_2) in weight percent.

The porosity of the specimens was assessed using MIP with a Micromeritics AutoPore IV 9500 porosimeter, capable of reaching a maximum pressure of approximately 34,000 psia and a minimum pressure of 0.5 psia. A surface tension of 480 mN/m was applied, and the contact angles for intrusion and extrusion were set at 130° and 104°, respectively, as described in (Ma, 2014). Prior to testing, the specimen samples were stored in a glass desiccator with silica gel for 24 h to remove moisture and ensure accurate results. The microstructure of the samples was observed using a ZEISS AURIGA scanning electron microscope (SEM).

XRD was determined with a Bruker D8 ADVANCE diffractometer model. The diffraction diagrams of disoriented powder to characterise the mineralogy of the total sample were obtained in an angular interval from 2 to 65°, a step size of 0.02°, and a time per step of 1 s. Semi-quantitative analysis was performed following the method of (Chung, 1975) and using Bruker EVA software.

Flexural strength testing was determined by three-point bending tests on unnotched beam specimens to quantify the fibre reinforcement's contribution, before and after cracking, as can be seen in Fig. 4. A Shimadzu model AGS-X 10 kN universal testing machine, equipped with a 10 kN capacity load cell according to EN 12467:2013+A2 (UNE-EN 12467, 2018), was used. The test was managed using a closed-loop system, with a loading rate of 1 mm/min. The maximum flexural strength of the composite material (also known as Modulus of Rupture, MOR) was determined using Eq. (1),

$$MOR = \frac{3P_{max}L}{2bh^2} \quad (1)$$

where Pmax represents the maximum load recorded, in N, L is the span length (100 mm), and b and h are the width and thickness of the cross-section, in mm, respectively. The Limit of Proportionality (LOP) was defined as the point at which the load-deflection curve stops behaving linearly. For brittle materials, this value is similar to the MOR; however, for composites with fibres, the LOP is lower than the MOR, depending on the amount of fibre.

The toughness Index (I_G), defined as the area beneath the force-displacement curve comprised from 0 to a post-failure load of 0,4 MOR, was established as the parameter to characterise the type of failure. A value > 1,00 represents a ductile failure, while a value < 1,00 represents a fragile failure.

The flexural stiffness (K) was determined from the load–deflection response within the elastic deformation range using Eq. (2), where ΔP and Δf represent the increments in load, in N, and mid-span deflection,

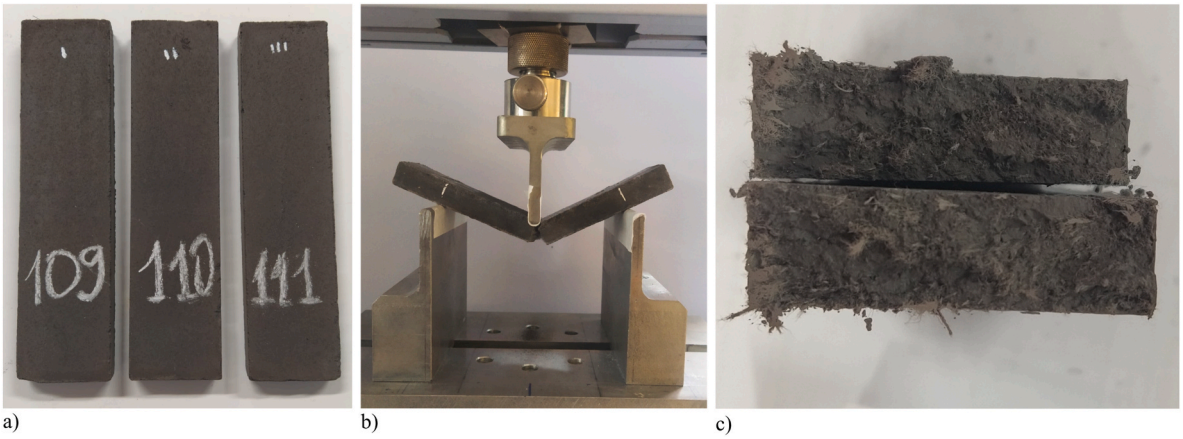

a) b) c)

Fig. 4. Flexural tests setup: (a) Fabricated specimens; (b) Specimens three-point bending test; (c) Cross-section of FRM specimens.

in mm, between two points within the linear regime. The remaining parameters are as previously defined in Eq. (1) (Sadrolodabaee et al., 2021b).

$$K = \frac{\Delta P.L^3}{4\Delta f.bh^3} \quad (2)$$

4. Experimental results

4.1. Carbonation results

The quantification of CO_2 uptake in carbonated composites was assessed via TGA, considering the mass loss associated with CO_2 release. Previous studies on steel slag carbonation report a release of CO_2 in the range of 500–850 °C, which corresponds to the thermal decomposition of calcium carbonate ($CaCO_3$), which is the main phase responsible for carbon capture in alkali-activated slag binders (Bonfante et al., 2024), (Liu et al., 2020), (Mo et al., 2016).

To calculate the amount of CO_2 absorbed during the carbonation process, the methodology proposed by (Grünhäuser Soares et al., 2022), (Bonfante et al., 2024), (Hu et al., 2022) was adopted. The total amount of CO_2 uptake during accelerated carbonation is commonly identified as the difference between the content of CO_2 before and after the carbonation referred to the initial mass of the so-treated material, the CO_2 uptake was estimated to follow Eq. (3) (Ferrara et al., 2023), (Huntzinger et al., 2009), (He et al., 2018).

$$CO_{2\ uptake}(\%) = \frac{M_1 - M_2 - M_3}{M_c} \quad (3)$$

Where: M1 is the residual mass before the decomposition of the carbonates; M2 is the residual mass after the decomposition of the carbonates; M3 is the mass of the initial CO_2 content in the non-carbonated material; and Mc is the mass of the material's binder (Grünhäuser Soares and Castro-Gomes, 2022).

Fibres are inert to CO_2, so the mass loss was normalised by 100 % EAFS, adjusting the presence of fibres, ensuring that the CO_2 absorption reflects only the carbonatable fraction of the mixture. The CO_2 uptake is often compared to the theoretical carbonation potential (TCO_2, wt%); this parameter represents the maximum potential for CO_2 fixation assuming complete conversion of CaO into $CaCO_3$. TCO_2 is obtained through Eq. (4) (Huntzinger et al., 2009) and calculated from the weight % of the EAFS oxide content resulting from the XRF analysis.

$$TCO_2(\%) = 0.785(CaO - 0.56 \times CaCO_3 - 0.7 \times SO_3) + 1.091 \times MgO + 0.71 \times Na_2O + 0.468\ (K_2O - 0.632 \times KCl) \quad (4)$$

The degree of carbonation can be calculated as the ratio between CO_2 uptake and TCO_2 of the material, according to Eq. (5) (Shi et al., 2012).

$$DCO_2(\%) = \frac{CO_{2\ uptake}(\%)}{TCO_2(\%)} \quad (5)$$

4.1.1. TGA-DTG

The results of the TGA and DTG analyses are presented in Fig. 5. The reference steel slag (EAFS) showed negligible weight loss within both intervals, confirming its low initial carbonation state and the absence of fibres. The postcarbonation fibre-free slag sample (S) presented an intermediate profile, while the presence of fibres appeared to enhance CO_2 uptake, as deduced from the increased mass loss between 500 °C and 850 °C in the fibre-reinforced composites. These observations confirm that both the fibre content and the carbonation curing process significantly influence the thermal decomposition behaviour of the studied

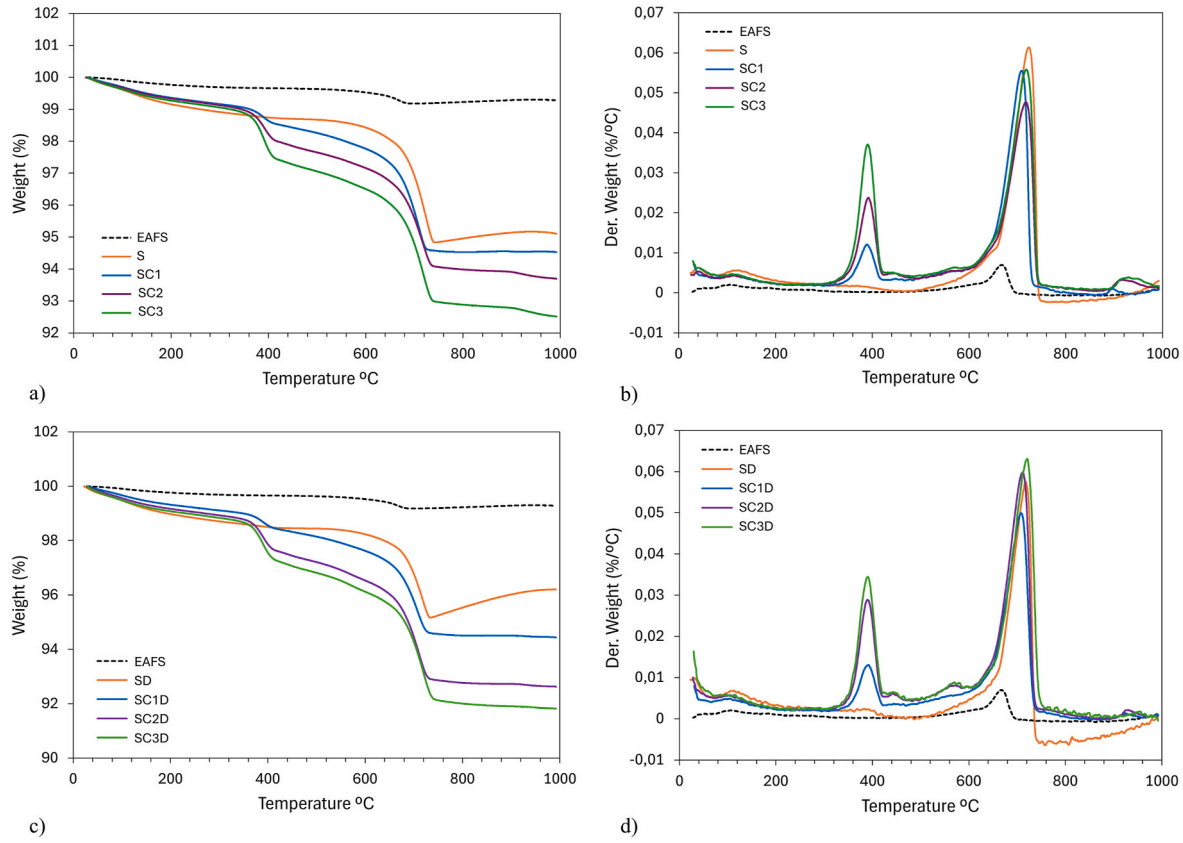

Fig. 5. TGA and DTG curves of carbonated slag-based composites with and without durability cycles: (a) TGA of unexposed specimens (S, SC1, SC2, and SC3); (b) DTG of unexposed specimens; (c) TGA of specimens after wet–dry durability cycles (SD, SC1D, SC2D, and SC3D); (d) DTG of specimens after wet–dry durability cycles.

composites.

Two principal mass loss events were identified in composites containing synthetic cotton fibres, corresponding to distinct thermal decomposition processes.

The first mass loss occurred within the temperature range of approximately 300–460 °C. This peak was more pronounced in samples with a higher fibre content (SC1, SC2, SC3), as reflected in both the TGA and DTG curves. This behaviour is attributed to the thermal degradation of textile fibres, primarily composed of cotton and polyester. The DTG peak within this interval was sharper and more intense for the sample containing 3 % fibre (SC3), confirming the influence of fibre dosage on this thermal event.

The second major mass loss event was recorded between 500 °C and 850 °C. This step is associated with the decomposition of carbonates, specifically calcium carbonate ($CaCO_3$), formed during the carbonation curing process. This interpretation aligns with the findings reported by (Bonfante et al., 2024) and (Capelo-Avilés et al., 2024), who employed the same temperature interval to quantify CO_2 uptake in steel slag-based carbonated binders. The DTG curves exhibited sharp peaks centred around 700–750 °C, characteristic of $CaCO_3$ decarbonation (Mo et al., 2016).

Beyond quantifying CO_2 uptake, thermal decomposition profiles provide information on the nature of the calcium carbonate phases formed. According to (Hu et al., 2022) and (Capelo-Avilés et al., 2024), amorphous calcium carbonate (ACC) tends to decompose at slightly lower temperatures (typically between 500 °C and 650 °C), whereas crystalline phases such as calcite and vaterite display decomposition peaks at higher temperatures, generally between 650 °C and 850 °C. In the present study, the DTG curves exhibit broad decomposition peaks spanning this entire range, suggesting the coexistence of both amorphous and crystalline carbonate forms. This observation is consistent with the carbonation mechanisms reported for alkali-activated slag systems, where initial carbonation may promote the formation of ACC, which subsequently transforms into more stable crystalline polymorphs with time (Bonfante et al., 2024), (Ashraf and Olek, 2018).

The TGA and DTG results for the mixtures subjected to wet-dry ageing cycles did not show significant changes, maintaining the same trend as that of the reference specimens not exposed to such cycles.

4.2. Porosimetry results

4.2.1. Results of the normal cured specimens

The porosity and pore structure analysis presented in Tables 3 and 4 reveal the influence of synthetic cotton fibre incorporation on the physical properties of carbonated EAFS-based composites. As can be observed in Table 3 for samples with incorporation, the microstructure is substantially modified, resulting in an increase in total porosity, average pore diameter, and critical diameter. There is a significant increase in porosity of 22 % and 33 % with the incorporation of 2 % and 3 % fibre. In addition, with the incorporation of fibres, the content of mesopores and macropores decreases, and the content of larger pores increases.

Table 3
Porosimetry results for samples.

Mixture Label		S	SC2	SC3
Porosity (%)		21.82	26.52	28.95
Bulk Density at 14.50 psia (g/mL)		2.63	2.57	2.35
Apparent (skeletal) Density (g/mL)		3.33	3.35	3.06
Average Pore Diameter (μm)		0.06	0.12	0.13
Critical diameter (μm)		0.35	0.68	1.05
Pores typology	Mesopores (0.002–0.05 μm)	15.70	8.20	7.90
	Macropores (0.05 μm–10 μm)	78.90	74.20	64.80
	Air voids/cracks (> 10 μm)	5.30	17.60	27.30

Bulk density exhibits an inverse relationship, with incorporations of 2 % and 3 % resulting in reductions of 2.3 % and 11 %, respectively, as the higher fibre volume fraction introduces supplementary air voids and larger pore structures. The most significant changes are in the values of average pore diameter and critical diameter, with increases of 100 % and 94 % for 2 % fibre and 117 % and 200 % for 3 % fibre.

Table 4
Porosimetry results for durability samples.

Mixture Label		SD	SC2D	SC3D
Porosity (%)		20.40	28.62	35.71
Bulk Density at 14.50 psia (g/mL)		2.74	2.53	2.28
Apparent (skeletal) Density (g/mL)		3.40	3.41	3.22
Average Pore Diameter (μm)		0.08	0.12	0.16
Critical diameter (μm)		0.55	1.33	2.08
Pores typology	Mesopores (0.002–0.05 μm)	11.70	8.00	6.50
	Macropores (0.05 μm–10 μm)	83.10	77.10	66.00
	Air voids/cracks (> 10 μm)	5.20	14.90	27.50

In terms of pore size distribution, a notable decrease in mesopores (0.002–0.05 μm) and macropores (0.05–10 μm) was observed as the fibre content increased. In contrast, the proportion of larger air voids/cracks (>10 μm) increased significantly. Furthermore, with the incorporation of fibres, the content of mesopores and macropores decreases and the air voids/cracks fraction (>10 μm) increased markedly from 5.3 % in S to 27.3 % in SC3, which may affect mechanical performance and CO_2 uptake capacity.

4.2.2. Results after being exposed to durability

Following wet-dry ageing cycles, these trends were accentuated, as can be observed in Table 4, leading to an increase in total porosity by 40 % with 2 % fibres and 75 % with 3 % fibres, much larger with the higher amount of fibres, SC3D. The increase in porosity is consistent with observations from studies such as (Zhuge et al., 2024) in which the addition of textile fibres was associated with an increase in interconnectivity in cementitious pastes. However, the pore size distribution is quite similar to that of natural specimens. Reductions in bulk density, along with increases in mean pore diameter and critical diameter, follow patterns similar to those observed in non-exposure to environmental cycles specimens.

4.3. Flexural strength results

The flexural performance results summarised in Table 5 and Fig. 6 reveal a differentiated response depending on the fibre dosage and exposure to wet-dry ageing cycles. For the unexposed specimens, the incorporation of synthetic cotton fibres at low dosages (1–2 % by volume) did not significantly enhance the flexural strength, as evidenced by MOR and LOP values that were similar to the reference sample (S). However, the I_G increased notably, rising from 0.75 kJ mm^2 for S to 2.07 kJ mm^2 for SC2, indicating an enhanced energy absorption capacity despite the matrix-dominated failure mode, and this is corroborated by the proximity between the MOR and LOP values in this case.

At a fibre dosage of 3 % (SC3), both the flexural strength and fracture energy improved substantially. The MOR increased to 6.09 N/mm^2 approximately 11 % higher than the reference, and the I_G reached 2.50

Table 5
Results of flexural strength of specimens with and without durability.

Mixture Label	*MOR (N/mm^2)*	*LOP (N/mm^2)*	*I_G (kJ·mm^2)*	*K Flexural stiffness (GPa)*
S	5.50 ± 1.27	5.50 ± 1.27	0.75 ± 0.16	3.43 ± 1.05
SC1	5.19 ± 0.17	5.19 ± 0.17	1.75 ± 0.07	3.09 ± 0.23
SC2	5.13 ± 0.67	5.01 ± 0.76	2.07 ± 0.26	2.68 ± 0.77
SC3	6.09 ± 0.35	5.14 ± 0.24	2.50 ± 0.14	3.12 ± 0.46
SD	4.76 ± 1.07	4.76 ± 1.07	0.94 ± 0.12	1.23 ± 0.52
SC1D	4.31 ± 0.17	4.31 ± 0.17	1.39 ± 0.34	1.77 ± 0.68
SC2D	4.24 ± 0.19	4.24 ± 0.19	1.38 ± 0.34	1.50 ± 0.78
SC3D	3.15 ± 0.15	3.01 ± 0.09	0.94 ± 0.14	0.73 ± 0.17

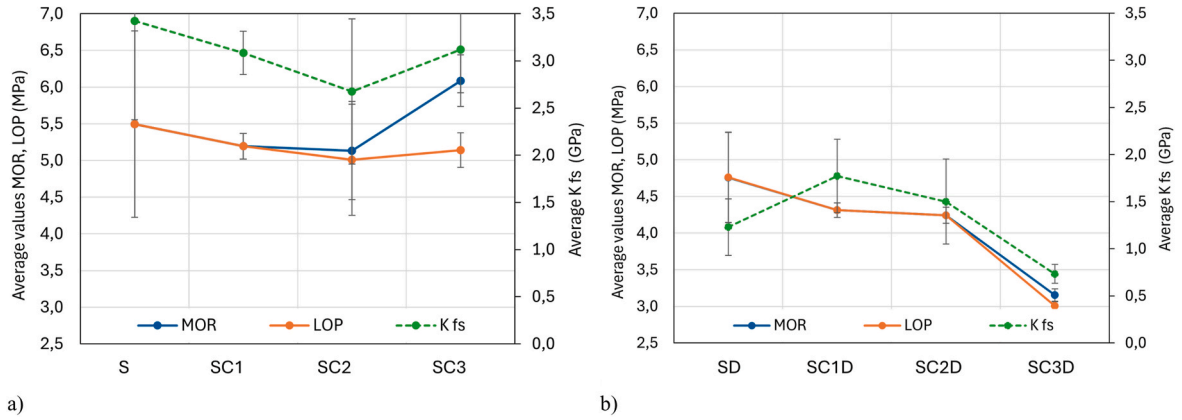

Fig. 6. Average values of MOR, LOP and K with standard error of carbonated slag-based composites with and without durability cycles: (a) unexposed specimens (S, SC1, SC2, and SC3); (b) specimens after wet–dry durability cycles (SD, SC1D, SC2D, and SC3D).

kJ mm^2, representing an overall improvement of more than 230 %. Furthermore, a more evident separation between LOP (5.14 N/mm^2) and MOR suggests that the fibres contributed to load bearing beyond matrix cracking. This behaviour aligns with (Sadrolodabaee et al., 2021b), where increased fibre volumes translated similarly into post-crack load transfer capacity and higher I_G values.

After exposure to wet–dry ageing cycles, a general reduction in mechanical performance was observed. For example, SC3D showed a reduction of approximately 48 % in MOR compared to SC3. The reference specimen (SD) exhibited an I_G of 0.94 kJ mm^2, whereas SC1D and SC2D maintained higher values (1.39 and 1.38 kJ mm^2, respectively), demonstrating partial retention of the reinforcement effect. In contrast, SC3D showed a marked decrease in I_G to 0.94 kJ mm^2, similar to the unreinforced specimen suggesting fibre deterioration and a loss of interfacial efficiency at high fibre dosages under cyclic exposure. The MOR and LOP results for the aged specimens further support this observation, indicating a reduced contribution of fibres to the post-cracking response after wet-dry ageing cycles.

As presented in Table 5, the non-reinforced matrices (S and SD) exhibited noticeably higher standard deviations in both MOR and LOP compared to the fibre-reinforced specimens. This behaviour is attributed to the manufacturing challenges related to the very low green strength of the without fibres material; small microcracks were often unavoidable due to the fragile state of the specimens. The incorporation of even a small amount of fibres, although not necessarily resulting in higher strength values, significantly improved workability, green stability, and the overall consistency of the specimens. The fibres promoted a more homogeneous stress distribution across the specimens, reducing sensitivity to localised microstructural defects.

4.4. SEM results

Scanning Electron Microscopy (SEM) was employed to analyse the fracture surfaces of selected specimens after flexural testing, in order to assess the morphology of the matrix and slag-based binder. SEM micrographs at 50 × and 300 × magnification for four representative samples are displayed in Fig. 7, specimens without fibres, S and SD, and Fig. 8, SC2 and SC2D, specimens with 2 % of synthetic cotton fibres.

Matrix S exhibited a relatively compact and homogeneous microstructure, with minimal visible defects or porosity. At this magnification (300 ×), the microstructure showed a rough surface texture and fine reaction products, which are characteristic of a well-carbonated matrix. After exposure to wet–dry ageing conditions, specimen SD apparently does not show any visible signs of degradation; as shown in Fig. 7a and b, both S and SD presented comparable morphologies, which aligns with the porosity and flexural strength results where both the MOR and LOP values remained practically unchanged. However, microcracks are appreciated in sample SD, which aligns with the reduced stiffness.

Fig. 7c and d provides the results of Scanning Electron Microscopy - Energy Dispersive X-ray Spectroscopy (SEM–EDX) at higher magnification (3000 ×). The elemental composition of sample SD was identified, revealing the presence of 27 wt% iron, 14 wt% calcium, 12 wt% carbon, 6 wt% manganese, and a significant proportion of oxygen. The significant iron content suggests that part of the FeO remained unreacted with CO_2, as iron oxides are far less reactive towards carbonation than calcium phases, which preferentially form stable $CaCO_3$.

The inclusion of fibres (SC2) introduced significant morphological heterogeneity on the fracture surface. At 50X, embedded fibres and fibre pull-out channels are clearly visible, suggesting effective load transfer and interaction with the matrix. The SEM images in 300X show textile fibres partially covered with carbonation products, as seen in Fig. 8 indicating good chemical bonding and possible nucleation of $CaCO_3$ on the fibre surface, which improve the fibre-matrix interface. This morphology supports the observed mechanical enhancement in flexural toughness and CO_2 uptake.

However, in the SC2D sample, after exposure to wet-dry aging conditions, significant microstructural degradation was observed. The matrix exhibited increased fragmentation and loss of structural cohesion, accompanied by increased porosity. The fibres appeared fractured, cracked, or partially detached from the matrix, and displayed noticeably shorter lengths (Fig. 8c and d) compared to those in the SC2 sample, confirming fibre degradation. The fibre–matrix interfacial zone showed clear signs of adhesion loss. These microstructural changes explain the decline in flexural strength and toughness observed after wet-dry ageing cycles and further confirm the detrimental effects of prolonged exposure to water and heat on both fibre integrity and matrix cohesion.

Overall, SEM observations confirm that the addition of fibres enhances matrix performance and carbonation efficiency in the short term, but also highlight the need to evaluate long-term stability, particularly under durability scenarios where fibre degradation and interfacial deterioration become critical factors.

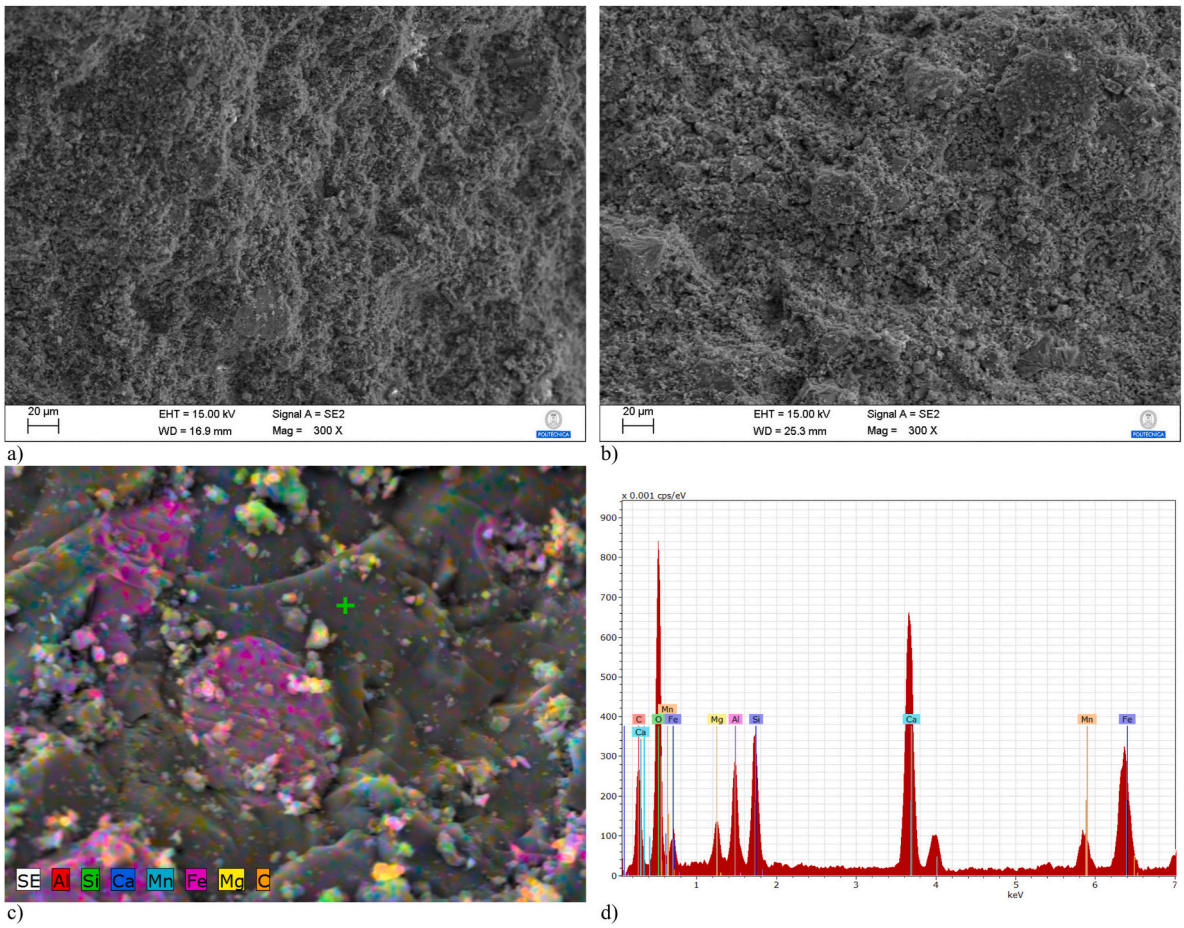

Fig. 7. SEM micrographs of the fracture surface: (a) S at 300X; (b) SD at 300X; (c) Mapping of specimen SD at 3000X; (d) SEM-EDX of specimen SD.

5. Discussion

5.1. Influence of the amount of fibre on CO_2 uptake

The influence of synthetic cotton fibre content on CO_2 uptake and carbonation degree (DCO_2) of EAFS-based composites is summarised in Table 6. The TCO_2 in EAFS was approximately 30.70 %, consistent with the values reported in the literature for similar compositions of slag from electric arc furnaces (Bonfante et al., 2024), (Capelo-Avilés et al., 2024). CO_2 uptake values ranged from 3.23 % to 4.65 % depending on fibre dosage and the curing conditions.

Fig. 9 shows that increasing the fibre content from 1 % (SC1) to 3 % (SC3) progressively improves CO_2 uptake, from 3.37 % to 3.97 % in the initial condition and up to 4.65 % after wet-dry ageing cycles. A similar trend is observed for the degree of carbonation (DCO_2), which increased from 10.52 % for the reference S mixture to 12.93 % for SC3 and further to 15.15 % for SC3D after exposure to environmental cycles. These results indicate that fibre inclusion not only acts as a passive filler but actively promotes carbonation processes. According to (Zhuge et al., 2024) the porous structure of natural fibres, such as cotton, generates additional pathways within the matrix, increasing the surface area exposed to carbonation reactions and favouring greater penetration of CO_2.

This behaviour may be attributed to the dual role of fibres; initially, fibres contribute to increased porosity and formation of the capillary network, facilitating CO_2 diffusion during curing. Over time, as confirmed in wet-dry ageing samples, fibre degradation is most likely through hydrolysis (Regazzi et al., 2016) leading to additional pore formation and thus increased access to CO_2. This two-stage carbonation enhancement, first through fibre-induced porosity and later through fibre degradation, is supported by TGA and porosity results, which show higher mass loss and increased air voids in samples with greater fibre content. The notable increments in the degree of carbonation after ageing conditions may be related to the formation of further hydration products, as can be seen in Section 4.4.

In general, these findings confirm that the presence of textile fibres in EAFS-based composites significantly enhances the potential for CO_2 sequestration, both immediately after cure and following exposure to environmental ageing conditions.

5.2. Influence of the fibre dosage on the porosity

The influence of synthetic cotton fibres on the pore structure of carbonated steel slag composites was analysed in detail based on mercury intrusion porosimetry (MIP) results (Fig. 10, Tables 3 and 4). In terms of pore size distribution, a notable decrease in mesopores (0.002–0.05 µm) and macropores (0.05–10 µm) was observed as fibre content increased. Mesopores reduced from 15.7 % in S to 8.2 % in SC2 and 7.9 % in SC3. Similarly, macropores decreased from 78.9 % in S to 74.2 % (SC2) and 64.8 % (SC3). On the contrary, the proportion of larger air voids/cracks (>10 µm) increased significantly, from 5.3 % in S to 17.6 % in SC2 and 27.3 % in SC3. This indicates that the fibres, while initially occupying space within the matrix without degrading, contribute to an increase in larger voids due to their spatial arrangement and interaction with the binder.

Following wet-dry cycles, these trends were accentuated. The SC2D and SC3D samples showed further increases in porosity and critical pore diameter, suggesting degradation or loss of the structural role. This is consistent with the hypothesis that fibres partially degrade under environmental stress, leaving voids that were initially filled.

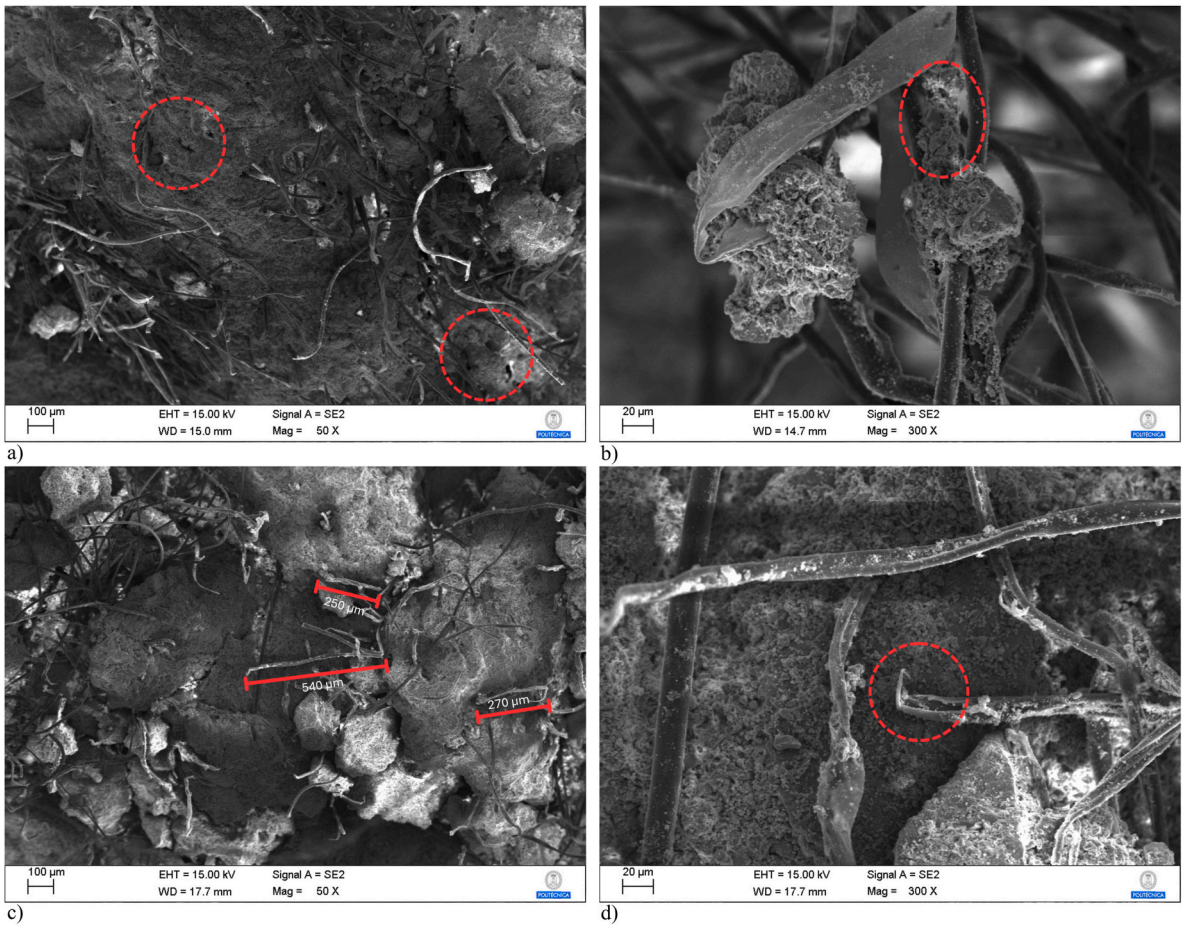

Fig. 8. SEM micrographs of the fracture surface: (a) specimen SC2 at 50X; (b) specimen SC2 at 300X; (c) specimen SC2D at 50X; (d) specimen SC2D at 300X.

Specifically, porosity increased from 20.40 % (SD) to 28.62 % (SC2D) and 35.71 % (SC3D), with the proportion of air void/crack rising to 14.9 % and 27.5 %, respectively as shown in Fig. 10. This behaviour may also be influenced by weakening of the fibre-matrix interface and microcrack development during carbonation curing and exposure to environmental cycles.

In conclusion, fibre incorporation modifies the pore structure by decreasing mesopore and macropore fractions while increasing larger air voids, a phenomenon that increases after exposure to ageing conditions, highlighting the dual effect of fibres as both reinforcement and pore structure modifier.

5.3. *Influence of the amount of fibre on flexural mechanical performance*

Fig. 11 illustrates a representative sample of the flexural mechanical behaviour of the carbonated slag-based composites. The initial slope corresponds to the elastic modulus of the material. With the incorporation of fibres, the composite still has the possibility to increase the strength until MOR is reached even with some microcracks in the matrix. After peak, major cracking occurs, and either there is a steep drop related to a brittle failure or a gradual decline related to ductile behaviour and energy dissipation through crack bridging or toughening mechanisms. Specimens undergoing durability cycles still present

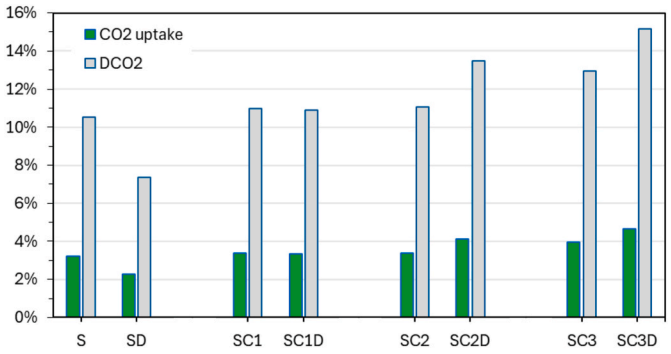

Fig. 9. CO_2 uptake and carbonation degree of mixture designs.

ductile behaviour, but slightly reduced tail length.

The results show a clear dependency on fibre content, affecting both pre-peak strength and post-peak ductility. At low fibre content (1 % by volume, SC1), the flexural strength parameters (MOR and LOP) did not show a significant improvement compared to the reference sample (S). As it was explained in Section 4.3, the incorporation of textile fibres markedly reduced the standard error of the mechanical results,

Table 6
Estimated CO_2 uptake, DCO_2 of mixture designs.

Mixture label	S	SC1	SC2	SC3	SD	SC1D	SC2D	SC3D
$CO_{2uptake}$ (%)	3.23	3.37	3.40	3.97	2.26	3.34	4.14	4.65
DCO_2 (%)	10.52	10.98	11.07	12.93	7.36	10.88	13.49	15.15

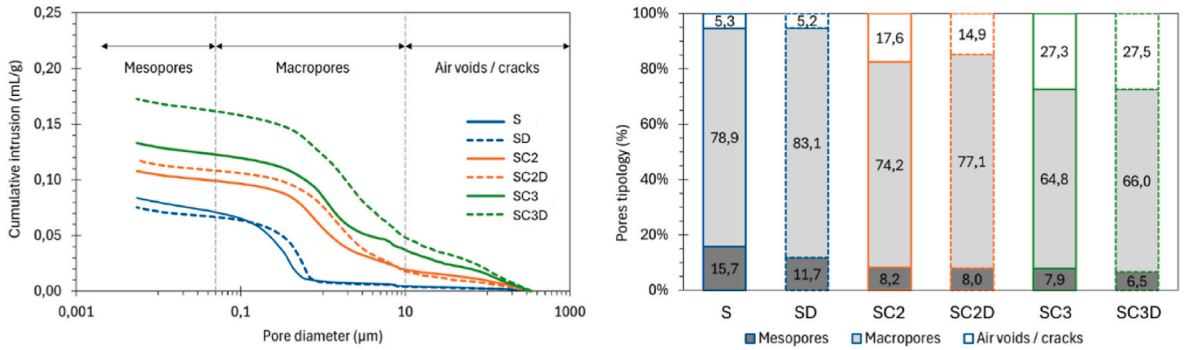

Fig. 10. Influence of the fibre dosage in the porosity.

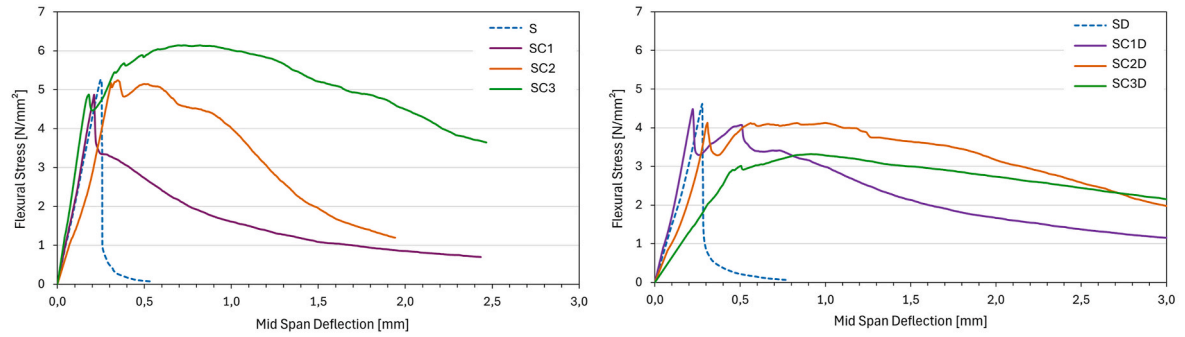

Fig. 11. Flexural mechanical behaviour of carbonated EAFS composites: (a) unexposed specimens (S, SC1, SC2, SC3); (b) specimens after wet–dry durability cycles (SD, SC1D, SC2D, SC3D).

achieving a reduction of approximately 80 % with fibres addition. Fibre-reinforced specimens exhibited a more consistent flexural response, with deviations in MOR and LOP decreasing by up to 87 % when comparing S with SC1, and by around 86 % when comparing SD with SC3D. This behaviour suggests that fibre-free specimens are more susceptible to microstructural defects such as pores and microcracks in the manufacture process.

Increasing the fibre content to 2 % and 3 % (SC2 and SC3) led to marked improvements in both pre-peak strength and post-peak behaviour. For SC3, the load-deflection curve demonstrates an extended post-peak tail, indicative of increased toughness and effective fibre-matrix interaction. The separation between LOP and MOR becomes more distinct at higher fibre dosages, signifying that fibres contribute not only to bridging cracks post-cracking but also to sustaining additional loads beyond the matrix fracture limit.

In terms of durability, exposure to environmental cycles (SD series) showed a general reduction in mechanical performance across all composites. This reduction is more relevant after the peak. However, composites with higher fibre dosages (SC2D and SC3D) retained greater residual strength and ductility compared to their low-fibre and fibre-free counterparts. Although fibre degradation likely occurred during durability exposure, the remaining fibres and the modified pore structure induced by their presence appeared to mitigate overall mechanical degradation.

5.4. *Influence of fibres dosage on the mineralogical phases*

The X-ray diffraction (XRD) patterns (Fig. 12) corroborate the TGA observations and provide further insight into the phase composition and degree of carbonation of the studied samples. Uncarbonated slag (EAFS) exhibits characteristic crystalline phases, including merwinite ($Ca_3Mg(SiO_4)_2$), gehlenite ($Ca_2Al_2SiO_7$), larnite (Ca_2SiO_4), magnetite (Fe_3O_4) and wuestite (FeO), as indicated by peaks 1, 4, 5, 6, and 7, respectively. These phases are consistent with the mineralogical profile of steel slags as reported by (Humbert et al., 2019), (Jiang et al., 2018), (Humbert and Castro-Gomes, 2019).

After carbonation curing, the samples S, SC2, and SC3 show the appearance and increase in intensity of the peaks associated with calcite ($CaCO_3$) (peak 3), indicating effective CO_2 uptake (Fig. 12b and d). In particular in the SC3 sample, the calcite peaks are markedly more pronounced, aligning with the greater mass loss observed in the TGA analysis between 500 and 850 °C. This suggests a higher degree of carbonation, corroborating the trend identified in the CO_2 uptake quantification.

Additionally, the persistence of quartz (SiO2) (peak 2) in all samples suggests that it remains unreacted during carbonation. This behaviour has been reported similarly by (Hu et al., 2022), (Ashraf and Olek, 2018) who observed that quartz phases in alkali-activated and carbonated slag-based composites maintain structural integrity, contributing to the physical matrix without undergoing carbonation-related changes.

It should be noted that in the carbonated samples, the peak broadening and reduced intensity of some crystalline phases (larnite and gehlenite) may also indicate partial amorphization or transformation into calcium carbonate phases. This observation is consistent with the findings of (Bonfante et al., 2024), (Capelo-Avilés et al., 2024) who associated similar changes in the XRD pattern with the coexistence of amorphous and crystalline calcium carbonate phases in carbonated steel slag systems. The authors highlight that such structural modifications reflect the dynamic nature of carbonation reactions, leading to phase transformation and possible reorganisation of the mineral matrix.

Alternating wet and dry conditions significantly affect carbonation behaviour. While not explicitly detailed in the previous references, it is known from carbonation research that cyclic exposure can deepen carbonation penetration. In a dry period, CO_2 gas can diffuse farther into the material; upon subsequent rewetting, that CO_2 dissolves and reacts with available Ca in the interior. This cyclical mechanism can gradually

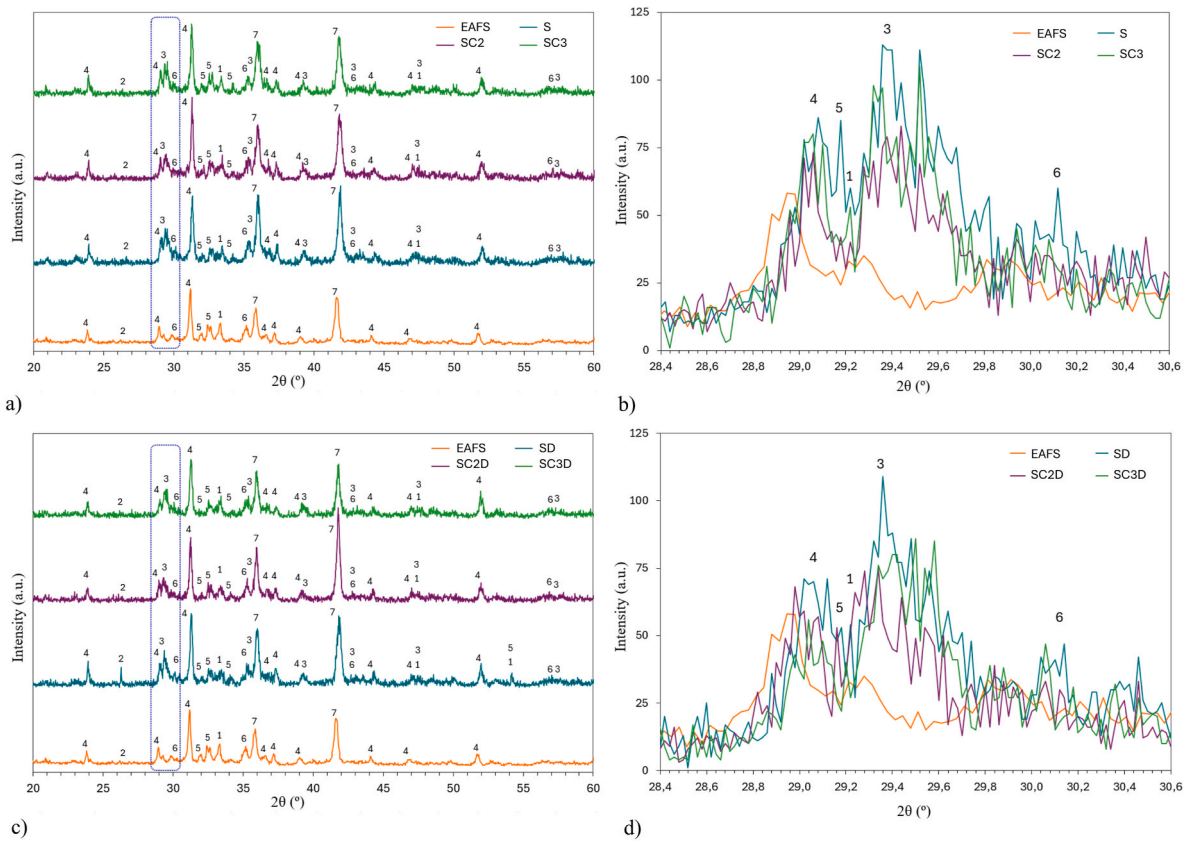

Fig. 12. XRD pattern: (a)(c) samples without durability cycles; (b)(d) samples of specimens exposed to durability cycles. Legend: 1 Merwinite ($Ca_3Mg(SiO_4)_2$); 2 Quartz (SiO_2); 3 Calcite ($CaCo_3$); 4 Gehlenite ($Ca_2Al_2SiO_7$); 5 Larnite (Ca_2SiO_4); 6 Magnetite (Fe_3O_4); 7 Wuestite (FeO).

carbonate phases like gehlenite that lie deeper in the matrix, beyond the reach of a continuously wet carbonation front. Additionally, drying out the material mobilises moisture from the pores (drawing it outward), then rewetting introduces fresh water that can carry CO_2 to previously uncarbonated zones. Essentially, cycles can overcome some self-arousing effects of carbonation. For instance, in steady-state curing, once a layer of calcite forms and pore moisture is consumed, carbonation slows or stops. But if a dry spell empties those pores and then new moisture with CO_2 comes in, a further reaction can occur behind the initial front. However, cyclic carbonation may also induce microcracks or dimensional changes due to repeating formation and drying of crystals (Chang et al., 2018), (Zhao et al., 2025).

6. Conclusions

This study investigated the impact of the incorporation of synthetic cotton fibres on CO_2 uptake and mechanical performance of steel slag-based composites subjected to accelerated carbonation. The main findings are as follows:

TGA identified two primary decomposition events: fibre degradation that occurs between 300 and 460 °C, and calcium carbonate decomposition between 500 and 850 °C. CO_2 uptake increased with fibre content, ranging from 2.26 % to 4.65 %, and from 7.36 % to 15.15 % in differential CO_2 uptake (DCO_2) for composites with 3 % fibre content under wet-dry cycling. This improvement is attributed to increased internal porosity and improved CO_2 diffusion pathways facilitated by the fibres. These results were supported by differential thermogravimetry (DTG) and X-ray diffraction (XRD), which showed increased calcite formation and a reduction in gehlenite and larnite signals, indicating phase transformation and partial amorphization due to carbonation. Mercury intrusion porosimetry (MIP) further confirmed these trends, revealing an initial reduction in the number of mesopores and macropores, as a result of the space-filling effect of the fibres, and an increment of larger air voids.

The addition of textile fibres also influenced the mechanical behaviour of the composites. While 1 % fibre content did not significantly enhance flexural strength, it improved the workability of fresh mixtures and green strength. Composites with 2 % and 3 % fibre content exhibited improved fracture resistance, increased flexural toughness, as indicated by higher values of I_G and K, and clear separation between the LOP and MOR, suggesting effective fibre bridging and post-cracking load-bearing capacity. For example, composites with 3 % fibre dosage result in a notable increase in MOR, 6,09 N/m^2, and improved post-cracking behaviour.

Cyclic wet–dry exposure was found to enhance carbonation. During dry periods, the CO_2 gas penetrates deeper into the material and, upon rewetting, it dissolves and reacts with the calcium available in the interior. This process mobilises pore moisture during drying and introduces fresh water during rewetting, allowing CO_2 to be transported to previously uncarbonated zones, enhancing the degree of carbonation to 15.15 %. In contrast to steady-state curing, where calcite formation and moisture depletion can halt carbonation, cyclic conditions allow carbonation to progress beyond the initial reaction front.

Mechanically, cyclic carbonation has a dual effect. Although it promotes the formation of additional carbonation products, it may also induce microcracking and dimensional changes as a result of repeated crystal formation and drying, altering prepeak behaviour and reducing MOR in composites with a high synthetic cotton fibre content. Furthermore, fibre degradation during wet–thermal ageing introduced new voids and altered pore connectivity, as evidenced by increased porosity and larger pore diameters. This degradation significantly affected post-peak behaviour, decreasing the flexural toughness provided by the fibres, especially at higher dosages.

In summary, incorporation of synthetic cotton textile waste fibres

into carbonated slag composites improves both CO_2 capture and mechanical performance under controlled conditions. However, long-term exposure to wet-dry cycles underscores the need to optimise fibre content to balance performance gains with resistance to matrix and fibre degradation. Despite reduction in mechanical properties after exposure to wet-dry cycles, fibre reinforced composites retained some ductility and energy absorption capacity, suggesting potential for non-structural or semi-structural applications where environmental exposure is a concern.

CRediT authorship contribution statement

Anabel Castillo-Rodríguez: Writing – original draft, Visualization, Methodology, Investigation, Formal analysis, Data curation, Conceptualization. **Antonia Pacios-Álvarez:** Writing – review & editing, Writing – original draft, Supervision, Investigation, Formal analysis, Data curation, Conceptualization. **João Castro-Gomes:** Writing – review & editing, Validation, Resources, Project administration, Funding acquisition. **Justo García-Navarro:** Writing – review & editing, Supervision, Resources, Methodology, Funding acquisition.

Declaration of competing interest

The authors declare the following financial interests/personal relationships which may be considered as potential competing interests: Anabel Castillo-Rodriguez, Antonia Pacios-Álvarez, João Castro-Gomes and Justo García-Navarro, reports financial support, and travel were provided by European Research Executive Agency.

Acknowledgments

This research was partially funded by the European Union, under the Horizon Europe Marie Skłodowska-Curie Actions Staff Exchange Programme, under the project "CSTO2NE – Biomimicry and carbon adsorbent eco-materials for a climate-neutral economy" (Grant Agreement No. 101086302). Views and opinions expressed are, however, those of the author(s) only and do not necessarily reflect those of the European Union or European Research Executive Agency. Neither the European Union nor the granting authority can be held responsible for them.

The authors acknowledge Harsco Environmental Portugal for kindly providing the electric arc furnace slag (EAFS) used in this research and Alcorcertex, S.L., Spain, for providing the waste textile fibres.

Data availability

Data will be made available on request.

References

Agency, E.E., 2024. Management of Used and Waste Textiles in Europe's Circular Economy.

Ashraf, W., Olek, J., 2018. Carbonation activated binders from pure calcium silicates: reaction kinetics and performance controlling factors. Cem. Concr. Compos. 93, 85–98. https://doi.org/10.1016/j.cemconcomp.2018.07.004.

Assi, L., Carter, K., (Eddie) Deaver, E., Anay, R., Ziehl, P., 2018. Sustainable concrete: building a greener future. J. Clean. Prod. 198, 1641–1651. https://doi.org/10.1016/J.JCLEPRO.2018.07.123.

Badara, O., Rämö, V., Rissanen, M., Tehrani-Bagha, A., 2025. Mechanically recycled textile fibers in carded and needle-punched non-wovens: implications on processability, structure, and performance. Textil. Res. J. 95 (13–14), 1617–1636. https://doi.org/10.1177/00405175241302482.

Biava, G., Depero, L.E., Bontempi, E., 2024. Accelerated carbonation of steel slag and their valorisation in cement products: a review. Spanish Journal of Soil Science 14 (April), 1–17. https://doi.org/10.3389/sjss.2024.12908.

Bonfante, F., Ferrara, G., Humbert, P., Garufi, D., Tulliani, J.M.C., Palmero, P., 2024. CO2 sequestration through aqueous carbonation of electric Arc Furnace slag. J. Adv. Concr. Technol. 22 (4), 207–218. https://doi.org/10.3151/jact.22.207.

Capelo-Avilés, S., et al., 2024. A thorough assessment of mineral carbonation of steel slag and refractory waste. J. CO2 Util. 82. https://doi.org/10.1016/j.jcou.2024.102770.

Chang, H., Mu, S., Feng, P., 2018. Influence of carbonation on 'maximum phenomenon' in surface layer of specimens subjected to cyclic drying-wetting condition. Cement Concr. Res. 103, 95–109. https://doi.org/10.1016/J.CEMCONRES.2017.10.005.

Chen, X., Memon, H.A., Wang, Y., Marriam, I., Tebyetekerwa, M., 2021. Circular economy and sustainability of the clothing and textile industry. Materials Circular Economy 3 (1), 1–9. https://doi.org/10.1007/s42824-021-00026-2.

Chung, F.H., 1975. Quantitative interpretation of X-ray diffraction patterns of mixtures. III. Simultaneous determination of a set of reference intensities. J. Appl. Crystallogr. 8 (1), 17–19. https://doi.org/10.1107/S0021889875009454.

Dellagi, A., Ayed, R., Skouri, S., Bouadila, S., Guizani, A.A., 2024. Analyzing recycled waste-infused mortars: preparation and examination of thermal, mechanical, and chemical characteristics. Constr. Build. Mater. 425 (October 2023), 135996. https://doi.org/10.1016/j.conbuildmat.2024.135996.

DiGiovanni, C., Hisseine, O.A., Awolayo, A.N., 2024. Carbon dioxide sequestration through steel slag carbonation: review of mechanisms, process parameters, and cleaner upcycling pathways. J. CO2 Util. 81 (March), 102736. https://doi.org/10.1016/j.jcou.2024.102736.

Dissanayake, D.G.K., Weerasinghe, D.U., Wijesinghe, K.A.P., Kalpage, K.M.D.M.P., 2018. Developing a compression moulded thermal insulation panel using postindustrial textile waste. Waste Manag. 79, 356–361. https://doi.org/10.1016/J.WASMAN.2018.08.001.

Echeverria, C.A., Handoko, W., Pahlevani, F., Sahajwalla, V., 2019. Cascading use of textile waste for the advancement of fibre reinforced composites for building applications. J. Clean. Prod. 208, 1524–1536. https://doi.org/10.1016/j.jclepro.2018.10.227.

Fang, Y., Su, W., Zhang, Y., Zhang, M., Ding, X., Wang, Q., 2022. Effect of accelerated precarbonation on hydration activity and volume stability of steel slag as a supplementary cementitious material. J. Therm. Anal. Calorim. 147 (11), 6181–6191. https://doi.org/10.1007/s10973-021-10914-z.

Ferrara, G., Belli, A., Keulen, A., Tulliani, J.M., Palmero, P., 2023. Testing procedures for CO2 uptake assessment of accelerated carbonation products: experimental application on basic oxygen furnace steel slag samples. Constr. Build. Mater. 406, 133384. https://doi.org/10.1016/J.CONBUILDMAT.2023.133384.

Grünhäuser Soares, E., Castro-Gomes, J., 2022. The role of biomass bottom ash in Carbonated Reactive Magnesia Cement (CRMC) for CO2 mineralisation. J. Clean. Prod. 380. https://doi.org/10.1016/j.jclepro.2022.135092.

Grünhäuser Soares, E., et al., 2022. Feasibility for co-utilisation of Carbonated Reactive Magnesia Cement (CRMC) and industrial wastes in circular economy and CO2 mineralisation. Constr. Build. Mater. 323 (Mar). https://doi.org/10.1016/j.conbuildmat.2022.126488.

Grünhäuser Soares, E., Castro-Gomes, J., Magrinho, M., 2024. Investigating key factors for superior CRMC-based mortars cured under CO2 pressurized environment. Constr. Build. Mater. 447 (Oct). https://doi.org/10.1016/j.conbuildmat.2024.138143.

He, P., Shi, C., Poon, C.S., 2018. Methods for the assessment of carbon dioxide absorbed by cementitious materials. Carbon Dioxide Sequestration in Cementitious Construction Materials 103–126. https://doi.org/10.1016/B978-0-08-102444-7.00006-X.

Hu, L., Chen, Z., Hu, J., 2022. Carbon sequestration, mechanical properties and carbonation kinetics of PP-Fiber-Reinforced cement-based composites with CO2-Curing treatment. Coatings 12 (9). https://doi.org/10.3390/coatings12091339.

Huang, X., Zhang, J., Zhang, L., 2024. Accelerated carbonation of steel slag: a review of methods, mechanisms and influencing factors. Constr. Build. Mater. 411 (December 2023), 134603. https://doi.org/10.1016/j.conbuildmat.2023.134603.

Humbert, P.S., Castro-Gomes, J., 2019. CO2 activated steel slag-based materials: a review. J. Clean. Prod. 208, 448–457. https://doi.org/10.1016/J.JCLEPRO.2018.10.058.

Humbert, P.S., Castro-Gomes, J.P., Savastano, H., 2019. Clinker-free CO2 cured steel slag based binder: optimal conditions and potential applications. Constr. Build. Mater. 210, 413–421. https://doi.org/10.1016/J.CONBUILDMAT.2019.03.169.

Huntzinger, D.N., Gierke, J.S., Kawatra, S.K., Eisele, T.C., Sutter, L.L., 2009. Carbon dioxide sequestration in cement kiln dust through mineral carbonation. Environ. Sci. Technol. 43 (6), 1986–1992. https://doi.org/10.1021/es802910z.

Jiang, Y., Ling, T.C., Shi, C., Pan, S.Y., 2018. Characteristics of steel slags and their use in cement and concrete—A review. Resour. Conserv. Recycl. 136, 187–197. https://doi.org/10.1016/J.RESCONREC.2018.04.023.

Key, S., Sugg, B., Dowling, F., Iranzo, A., Gray, S., 2023. Analysis of Waste Arisings in the Textiles Life Cycle. Wrap, pp. 1–70, 2024.

Lakshmaiya, N., Udhayakumar, G., Sathiyamurthy, S., Nadh, V.S., Maranan, R., Mammo, W.D., 2025. Multi-functional natural fiber composites using flaxseed and cotton: tailoring acoustic, mechanical, and thermal properties for eco-friendly applications. Discov. Appl. Sci. 7 (8). https://doi.org/10.1007/s42452-025-07345-y.

Liu, G., Schollbach, K., van der Laan, S., Tang, P., Florea, M.V.A., Brouwers, H.J.H., 2020. Recycling and utilization of high volume converter steel slag into CO2 activated mortars – the role of slag particle size. Resour. Conserv. Recycl. 160 (Sep). https://doi.org/10.1016/j.resconrec.2020.104883.

Ma, H., 2014. Mercury intrusion porosimetry in concrete technology: tips in measurement, pore structure parameter acquisition and application. J. Porous Mater. 21 (2), 207–215. https://doi.org/10.1007/s10934-013-9765-4.

Mo, L., Zhang, F., Deng, M., 2016. Mechanical performance and microstructure of the calcium carbonate binders produced by carbonating steel slag paste under CO2 curing. Cement Concr. Res. 88, 217–226. https://doi.org/10.1016/J.CEMCONRES.2016.05.013.

Park, C., Lee, J., 2024. Transforming biowaste into sustainable supplementary cementitious materials. J. Build. Eng. 98 (July), 110976. https://doi.org/10.1016/j.jobe.2024.110976.

Rahman, S.S., Siddiqua, S., Cherian, C., 2020. Sustainable applications of textile waste fiber in the construction and geotechnical industries: a retrospect. Clean. Eng. Technol. 6, 100420. https://doi.org/10.1016/j.clet.2022.100420, 2022.

Regazzi, A., Corn, S., Ienny, P., Bénézet, J.C., Bergeret, A., 2016. Reversible and irreversible changes in physical and mechanical properties of biocomposites during hydrothermal aging. Ind. Crops Prod. 84, 358–365. https://doi.org/10.1016/j.indcrop.2016.01.052.

Sadrolodabaee, P., Claramunt, J., Ardanuy, M., de la Fuente, A., 2021a. Characterization of a textile waste nonwoven fabric reinforced cement composite for non-structural building components. Constr. Build. Mater. 276, 122179. https://doi.org/10.1016/j.conbuildmat.2020.122179.

Sadrolodabaee, P., Claramunt, J., Ardanuy, M., de la Fuente, A., 2021b. Mechanical and durability characterization of a new textile waste micro-fiber reinforced cement composite for building applications. Case Stud. Constr. Mater. 14 (Jun). https://doi.org/10.1016/j.cscm.2021.e00492.

Shi, C., Meng, L., Pingping, H., Z, Ou, 2012. Factors affecting kinetics of CO2 curing of concrete. J Sustain Cem Based Mater 1 (1–2), 24–33. https://doi.org/10.1080/21650373.2012.727321.

Wang, C., et al., 2023. A sustainable strategy to transform cotton waste into renewable cellulose fiber self-reinforcing composite paper. J. Clean. Prod. 429. https://doi.org/10.1016/j.jclepro.2023.139567.

Wijesinghe, K.A.P., Gunasekara, C., Law, D.W., Hidallana-Gamage, H.D., Wanasekara, N., Wang, L., 2024. Thermal and acoustic performance in textile fibre-reinforced concrete: an analytical review. Constr. Build. Mater. 412 (January), 134879. https://doi.org/10.1016/j.conbuildmat.2024.134879.

Woodall, C.M., McQueen, N., Pilorgé, H., Wilcox, J., 2019. Utilization of mineral carbonation products: current state and potential, 9 (6), 1096–1113. https://doi.org/10.1002/ghg.1940.

Xia, G., et al., 2025. Complete recycling and valorization of waste cotton-spandex blended fabrics into value-added UV-blocking cellulose/graphene films and transparent polyurethane film. Sustain. Mater. Technol. 43 (Apr). https://doi.org/10.1016/j.susmat.2025.e01234.

Zhao, Z., Oh, D., Kitagaki, R., Zheng, T., Maruyama, I., 2025. Effect of Wet−dry cycles and water-to-cement ratios on cement paste carbonation. J. Adv. Concr. Technol. 23 (4), 205–222. https://doi.org/10.3151/jact.23.205.

Zhuge, Y., Ong, P.B., Wong, H.S., Myers, R.J., 2024. Natural fibre-enhanced CO2 transport and uptake in cement pastes subjected to enforced carbonation. J. CO2 Util. 90 (Dec). https://doi.org/10.1016/j.jcou.2024.102983.

Textile waste by numbers. Textile waste by numbers: socking facts that you need to know [Online]. Available. https://picvisa.com/textile-waste-recycling/#:~:text=Somecountriesperformbetter,isrecycled. (Accessed 2 July 2025).

UNE-EN 12467, 2018. UNE-EN 12467:2013+A2, fibre-cement Flat Sheets – Product Specification and Test Methods.